IOP Publishing *Mater. Res. Express* **13** (2026) 186401 https://doi.org/10.1088/2053-1591/ae9e0f

Materials Research Express

Check for updates

OPEN ACCESS

RECEIVED
29 March 2026

REVISED
8 July 2026

ACCEPTED FOR PUBLICATION
24 August 2026

PUBLISHED
16 September 2026

PAPER

A case study comparison of strain measurements in micromechanical testing using optical flow and DIC

Damian Lauria[1] and **Li-Anne Liew**[2,*]

[1] Office of Information Systems Management, National Institute of Standards and Technology, Boulder, CO 80305, United States of America

[2] Applied Chemicals and Materials Division, National Institute of Standards and Technology, Boulder, CO 80305, United States of America

[*] Author to whom any correspondence should be addressed.

E-mail: li-anne.liew@nist.gov and damian.lauria@nist.gov

Keywords: micromechanical testing, micro electro mechanical systems, strain measurement, optical flow, microtensile test, microshear test, LIGA

Abstract

We describe a case study on the application of an Optical Flow algorithm, using predictive velocity and pyramidal search, to the measurement of displacements in two 200 μm thick metal test specimens, compared with a traditional digital image correlation (DIC) implementation. One mesoscale tensile specimen and one mesoscale shear specimen of commercially fabricated electrodeposited nickel alloys, used in Micro Electro Mechanical Systems applications, were tested to fracture. The specimens were 200 μm thick and had gauge widths of 200 and 600 μm. Optical micrographs were taken during the tests. Displacements, strains, and mechanical properties were measured from the same sets of images using Optical Flow versus traditional DIC. The engineering stress–strain curves and shear stress vs shear strain curves from both techniques were similar (to within 1% for the engineering strains and 4%–9% for the shear strains) from the start of the tests to failure. This case study thus suggests Optical Flow shows promise as a measurement tool to complement DIC for mesoscale testing and warrants further investigation with more specimens. Potential advantages provided by Optical Flow in general include increased robustness and the potential for lower image segment search time, which could be especially beneficial for micro- and mesoscale test specimens.

1. Introduction

1.1. Micro- and mesoscale mechanical testing

The mechanical properties of structural materials are critical for engineering applications, as well as for scientific investigations into material behavior and new material development. Mechanical testing entails designing and fabricating test coupons, or specimens, of predetermined geometries, from the material under consideration, and subjecting them to controlled loads while the specimen's physical response—typically the deformation—is measured. Different specimen geometries and loading conditions are designed to induce different stress states in the material. Specimen sizes span many orders of magnitude, from meters down to a few nanometers in length, width, and thickness, depending on the type of material and the objective of the investigation.

The past four decades have seen increasing need for, and interest in, test specimens in the micro- and mesoscale size range. While no universal size definition exists, we define the 'mesoscale' as characteristic lengths from about 1 mm down to tens of micrometers, and the 'microscale' as being an order of magnitude smaller. Many researchers, however, refer to what we call the mesoscale size range as the microscale, and/or the millimeter size as the mesoscale, while other researchers define the microscale as encompassing 1 μm to 1 mm. Furthermore, it is not uncommon in the literature for the terms 'micromechanical testing' to be used synonymously with mesoscale tests. For example, the reviews in [1–7] show this mix of size definitions. Regardless of the terminology, the physical size distinction between

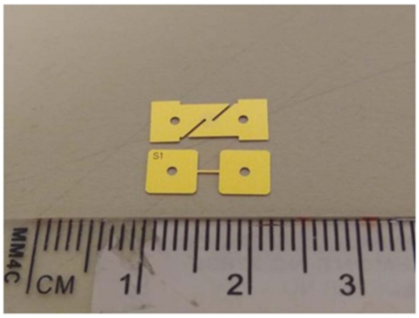

Figure 1. Photograph of 200 μm-thick tensile and shear specimens of electrodeposited nickel alloys in the present study, beside a millimeter ruler. The specimens were made in a commercial LIGA process. The tensile specimen is of a high-strength nanocrystalline Ni-10% Fe alloy. The shear specimen is of a more ductile micrograined Ni-10% Co. Details of the materials, specimen designs, fabrication processes, and their mechanical properties measured using traditional DIC, are in [12, 14].

specimens with characteristic lengths of $\sim$ 1 micrometer (μm) versus hundreds of micrometers—i.e. what we call the micro- vs mesoscales—impact some aspects of the experimental approaches. See [1–7] for reviews of micro and mesoscale mechanical test methods, which include both on-chip microfabricated actuators for load application and sensing, as well as tabletop or miniaturized off-chip test apparatuses and *in-situ* testing in scanning electron microscopes. Both the micro- and mesoscales are pertinent to micromechanics investigations since the displacements and deformations are on the order of micrometers.

Figure 1 shows two mesoscale specimens used in the present study: a tensile dog bone specimen and a shear specimen, both of 200 μm-thick electrodeposited nickel alloys used in Micro Electromechanical Systems (MEMS) applications and fabricated using a commercial LIGA process [8–11]. The details of the materials, specimen designs, test setups, test and analysis procedures, and measured mechanical properties, are available elsewhere [12–16].

The motivations for studying micro- and mesoscale specimens are generally three-fold: (1) For structural components of this size, the material properties should be measured from similar sized specimens to avoid size effects and manufacturing-induced material differences. Examples include MEMS and semiconductor devices and package components, for which structural components have dimensions ranging from 0.1 μm to 1 mm. The specimens in figure 1 fall into this category. (2) For obtaining spatially localized data for fundamental investigations into the behavior of larger materials. In this case, the structural component may be many orders of magnitude larger than the specimens but contains microstructural features and heterogeneity at the micro- or mesoscale which impact the material properties and behavior. Such features may include chemical or microstructural gradients, defects induced in manufacturing or in-service, or the interface of joined components such as in welds and additively manufactured alloys. Conventionally sized specimens represent an aggregate of the microstructural features. Therefore, micro- and mesoscale specimens are also needed to obtain localized information. Previous work also measured highly localized stress–strain curves of bulk additively manufactured metal alloys, by cutting mesoscale specimens, of identical geometry to the tensile specimen in figure 1, from bulk material [17, 18]. (3) For materials where mesoscale specimens are representative of bulk properties, the small size facilitates environmental testing, *in-situ* testing, or testing of in-service materials where there is limited material available. For example, the nuclear materials industry has long utilized small specimens for *in-situ* testing in test reactors, although those specimens are about 1–2 orders of magnitude larger than in our present study.

1.2. Displacement measurements in micro- and mesoscale testing

Central to all mechanical tests are displacement measurements. For micro- and mesoscale specimens, the displacements can range from a nanometer to hundreds of microns. Traditional extensometers are too large thus non-contact methods are used, most common are laser-based techniques such as laser interferometry, the interferometric strain/displacement gauge method [19], or commercial laser-based sensors. These techniques, however, are usually limited to one-dimensional strain measurement. Another non-contact measurement approach is digital image correlation (DIC), in which a sequence of images is captured while the specimen is deformed during a test and then analyzed to determine the displacements. DIC was developed in the 1980s for conventional or macroscale mechanical- and civil-engineering applications and is now a standard approach in these fields. It has been gaining interest more recently for

Table 1. General comparison between DIC and optical flow.

DIC	Optical flow
Developed by/for experimental solid mechanics	Developed by/for computer vision for motion tracking
Registration of images using correlation functions and iterative search strategies based on pixel brightness or Fourier transforms of the brightness values	Registration of images using derivatives of pixel brightness intensity, motion, and an estimate of future locations based on past optical flow velocities
Displacements usually calculated relative to first image	Displacements usually calculated relative to previous image, but larger timesteps can be used
Major applications: standard/default method for deformation measurement in solid mechanics	Major applications: object identification, motion tracking, image segmentation
Commercial programs geared to experimental solid mechanics (e.g. includes strain calculations)	Rarely applied in the field of experimental solid mechanics

experimental micromechanics studies. Unlike laser-based methods, image-based methods enable measurement of full-field strains in addition to localized and global strains, as well as measurements of crack initiation, nucleation and growth. Furthermore, the same set of images can be used for all the above. Image-based methods therefore provide a greater abundance of data, especially for investigations of material plasticity and fracture. A comprehensive review of DIC fundamentals is in [20] and a recent review is in [21].

In previous work, a classical DIC approach was used to measure strains on 200 μm-thick electrodeposited LIGA nickel alloys used in MEMS applications [12–16], as well as on 200 μm-thick specimens of bulk additively manufactured IN718 [18] and Ti-6 V-4Al [17]. The tensile specimens in these previous works were similar in size and geometry to the tensile specimen in figure 1.

A challenge with traditional DIC on small-scale specimens in general is the requirement for a suitable pattern of random, contrasting light and dark regions on the surface of the specimen. In conventional macroscale tests with large specimens such a pattern is typically achieved by spray painting the specimen's surface. Surface preparation is much more challenging for specimens under a millimeter in size. For micro- and mesoscale specimens, the most common approach is to use the natural surface texture as the pattern, as was done with the mesoscale specimens cut from additive manufactured alloys [17, 18]. However, for many specimens the surface texture may not be suitable for DIC. Many researchers have developed methods to apply micro- and nanoparticles, as well as other techniques such as focused ion beam milling, to the specimen surfaces to create patterns for DIC. Recent reviews of micro-patterning approaches for small specimens can be found in [6, 7]. An alternative approach used in the previous works on electrodeposited nickel alloys [12–14] centered on microfabricating thin-film Au dots with an engineered pattern on the mesoscale specimen surfaces to function as fiducial markers for DIC [13]. These microengineered fiducial markers were also fabricated on the surfaces of the specimens in figure 1. Even so, the fiducial markers may become more difficult to track during large deformations such as in the neck region of a tensile specimen, due to the increased motion as well as surface distortions resulting in changes in the lighting from the optical system. Image analysis techniques which have the potential for increased robustness and computational efficiency over classical DIC, could thus offer advantages for testing micro- and mesoscale specimens.

1.3. Application of optical flow in mechanical testing of materials

Another promising group of image-based techniques for measuring strains is Optical Flow, which was developed by and for the field of computer vision for motion tracking. Optical flow algorithms include a predictive step that calculates the previous velocity vector of the image segments being tracked and then uses that information to predict the next location to begin searching for that image segment. This predictive step can facilitate tracking even when subsections undergo considerable displacement from frame to frame, including moving beyond the bounds of the entire segment from the previous frame. Table 1 compares DIC to Optical Flow. Optical Flow feature-tracking algorithms incorporate a predictive element not typically seen in DIC that helps to reduce the search space and computation time needed to correlate a segment to a larger image. This predictive element is usually combined with pyramidal search strategies that further reduce the computational time needed for registration. The combination allows for segments to be tracked over greater time steps or with more movement from frame to frame without the need for an expanded search window.

Optical Flow to date is much less commonly used for mechanical testing of materials. Some examples are in [22–25]. These studies all utilized conventional-sized (macroscale) test specimens. Luo *et al* [22] developed a stereo-vision technique for measuring three-dimensional deformations of an object and demonstrated the application on tests of a cantilever beam and 304L stainless steel compact-tension specimen. Chivers and Clocksin [23] developed an optical flow algorithm and demonstrated it on tensile tests of Al 2024, and compression tests of carbon fiber composites. Hartmann *et al* [24, 25] compared DIC and Optical Flow for strain measurements of sheet metal undergoing large deformation and shear cutting. From the displacements they calculated the Von Mises equivalent strains and found that both measurement techniques provided similar global strains but with local differences.

Advanced methods of DIC have been developed that focus on the issue of decorrelation, where the algorithm becomes unable to reliably track image segments because of significant deformations or abrupt discontinuities [26, 27]. For Example, Pan *et al* [28] suggest a predictive estimation of motion and deformation that allows correlation to be maintained through periodic adjustment of the reference image. These improved DIC techniques can help to maintain correlation as the specimen under test deforms and the image segments distort. These methods generally require relatively small frame-to-frame displacements and may lose the ability to track altogether if displacements become larger than a fraction of the size of the segment.

When image segments move rapidly, some additional step is needed to ensure that the search area includes the segment being tracked. Without some method for accurately predicting where the image segment will be found, computationally expensive search of an expanded area is needed in order to maintain correlation. Optical flow solves this problem by predictively setting the initial search area for correlation. If the magnitude and direction of image segment movement is similar between subsequent frame pairs, then the Optical flow approach can potentially reduce search time and help to maintain tracking. Note that although a traditional DIC implementation was used in the present case study, the predictive search offered by Optical Flow does not preclude the use of more modern correlation methods.

1.4. Application of optical flow in micromechanical testing of materials

In this paper we describe a case study where Optical Flow was applied to deformation measurements in experimental *micro*-mechanics of materials. We compare the results to a classical DIC approach for one tensile specimen and one shear specimen of 200 μm-thick electrodeposited nickel alloys (figure 1). We compare Optical Flow to a classical DIC approach rather than to a more modern and advanced DIC approach because the previous works on these specimens [12, 14] used traditional DIC, and in this work we re-analyzed the same set of images from two of the specimens in [12, 14] but with Optical Flow. The displacements ranged from about 2 μm in the linear elastic region, to 300 μm at fracture. We now describe our Optical Flow technique and compare the results to that obtained from classical DIC on the same images in the previous work [12, 14, 29].

2. Optical flow approach vs DIC

A variety of methods can be employed in the implementation of two-dimensional (2D) DIC algorithms. In general, however, DIC algorithms employ some scheme to segment the image to be searched. DIC then implements one of several correlation criteria that allow an iterative search to find the best match in some template segment that maximizes similarity to the corresponding segment in the original image [21]. Typically, the correlation criteria will either compare the brightness intensity of the pixels in a 2D segment from the original image to those in the target image, or they will apply a Fourier transform and compare the intensity frequencies of the two images [30]. Sub-pixel accuracy can be achieved by selecting an appropriate approach for interpolation of the data to be correlated [21, 30].

A traditional DIC method was used to measure strains in the prior works on the 200 μm-thick specimens of Ni-10%Fe and Ni-10%Co alloys [12, 14]. The results reported in those studies form the basis for comparison in the present case study. The DIC approach relied on a stepwise search of a segment in the target frame for the point of minimum chi squared error of pixel brightness intensity displacements with respect to a template segment taken from the first frame. The area searched was simply the last known location where the template image was found, so it would lose the ability to track any region that moves more than half its own width in a single time step. The Marquardt–Levenberg algorithm was used to optimize the fit using bicubic interpolation for sub-pixel accuracy [31–33].

The choice of correlation criteria and search algorithm can have a profound effect on the efficiency of the overall DIC algorithm. An exhaustive, ordered search of an entire image is computationally wasteful if the likely location for the segment in question can be determined so that a smaller subset of the target image can be searched [34]. If the corresponding segment in the target image overlaps the bounds of the segment in the original image, or a sufficiently accurate guess can be made for its location, then correlation can be maximized using a 'hill climbing' approach. Otherwise, the target segment must be found through a more exhaustive search, if it can be found at all. DIC can be further complicated by the deformation of the surface being measured. Rotation, stretch, and skew are all possible for each segment in addition to the expected translation. Any correlation criteria chosen will need to be able to account for these transformations or it will only be able to track portions of the target surface that do not experience excessive deformation [35]. Traditional 2D DIC algorithms do best when the time step between images is small and the deformation in the tracked surface takes place incrementally and only in the plane of the image.

Optical flow techniques were developed to be a robust way of tracking the movements of objects across a visual field. Unlike traditional DIC algorithms, optical flow incorporates a time component and computes the 2D velocities of the segments within a pair of images in the plane of the image. Optical flow is only a measure of the velocities of image segments in the plane of the image, so it is not a true measure of velocity in a three-dimensional scene. In our experimental setup however, all motion in the specimen takes place in the same plane as the image, so the optical flow is a measure of the velocity of each segment being tracked.

The optical flow implementation used in this study uses Bouguet's [36] pyramidal implementation of the Lucas–Kanade registration algorithm [34]. The Lucas–Kanade feature tracker requires small displacements between the pixels in the template segment and the image being searched because it uses a first order Taylor expansion to estimate the derivatives of the pixel motions. Even with small displacements, some iterative registration may be necessary, which is accomplished using a Newton-Raphson iteration [34, 36]. The Lucas–Kanade method has the capability to handle linear distortions and changes in rotation between the template being matched and the corresponding segment in the frame being searched [34], which makes it a good candidate for strain measurements where a certain amount of distortion is expected. In principle, any correlation criteria could be substituted during the final registration step while still preserving the computational savings from the pyramidal search and velocity-based location prediction.

Rather than rely on an exhaustive search of all or part of the target image for a segment of the original image, this implementation of an optical flow algorithm uses the pyramidal search strategy laid out in [36]. This strategy uses a series of lower resolution images calculated from the original to track movements, by estimating motion in increasingly detailed versions of the image being searched. Each successive representation of the image uses higher resolution and therefore a more detailed estimation of the motion within the image.

At each timestep, the previous step's velocity information is then used as an initial guess for the segment's location in the new frame. Estimating this location using velocity allows for a prediction that is accurate enough that the subsequent correlation can often be accomplished in a single iteration [37]. The accuracy of the velocity component in making an initial guess also allows the algorithm to maintain efficient tracking even when there is significant movement of the image segments from frame to frame. Consequently, it can track faster deformations or use larger time steps than traditional DIC methods while maintaining higher computational efficiency.

3. Results: application to mesoscale mechanical testing and comparison to DIC

3.1. Mesoscale tensile tests

Previous work reported the elastic-plastic properties of 50 specimens of electrodeposited nickel alloys made from a commercial LIGA MEMS process, using a traditional DIC approach to measure the strains [12]. The 200 μm-thick Ni-10% Fe and Ni-10% Co films were fabricated into tensile specimens with gauge section lengths ranging from 1 mm to 3 mm, and gauge widths ranging from 75 μm to 700 μm. Details of the materials, specimen designs, specimen fabrication process, test apparatus, testing and analysis procedures, and the final measured tensile properties including size- and strain-rate effects, are described in [12, 13], and the materials' fracture behavior is described in [15]. Since the strains were measured using traditional DIC [30] of the optical micrographs, the same micrographs were reanalyzed in the present case study using the Optical Flow approach, for one specimen.

Figure 2 shows optical micrographs of one tensile specimen from the previous study and is a close up of an identical specimen to figure 1. This material was nanocrystalline Ni-10% Fe, with gauge dimensions 200 μm wide $\times$ 200 μm thick $\times$ 2 mm long. The dots are 1 μm-thick Au and were designed to function as fiducial markers for DIC [13] and now are used as fiducial markers for the optical flow program.

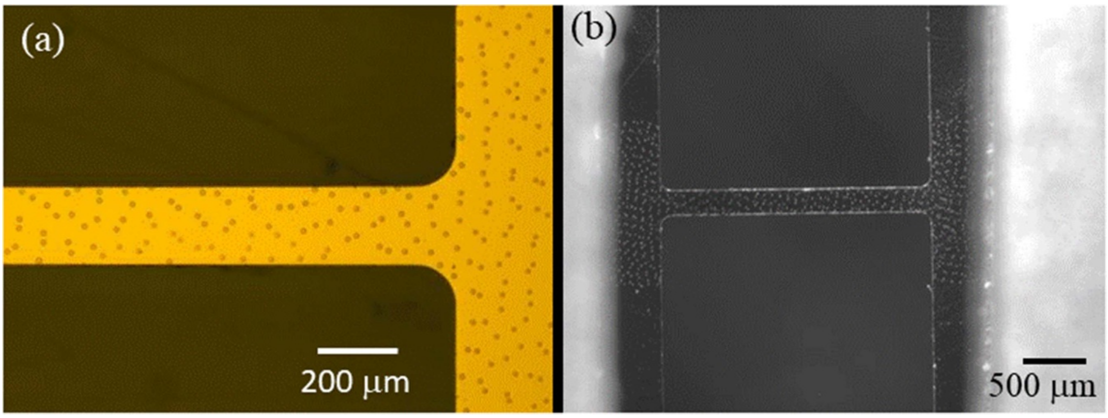

Figure 2. Optical micrographs of a mesoscale tensile specimen, 200 μm-thick, of nanocrystalline electrodeposited Ni-10% Fe, showing the pattern of microfabricated thin film gold dots used as fiducial markers for DIC and Optical Flow displacement measurement. Reproduced from [12]. © IOP Publishing Ltd. All rights reserved. (a) Optical micrograph showing the fiducial markers in detail. (b) Optical micrograph from the tensile test, at the start of the test.

This specimen was among 50 similar specimens analyzed with traditional DIC in the previous study [12]. The images of the tensile test were 3072 × 2300 pixels. We reanalyzed the images with the Optical Flow algorithm, using similar user-selected parameters as in the DIC program, as follows: The corresponding subsets in each program had the same initial coordinates. Subset sizes of 30–32 pixels were used, with one subset placed at each end of the gauge section.

Figure 3 compares the raw displacements measured by both programs, for the left and right ends of the gauge section, in the axial direction (the direction of stretch) and the transverse direction. As shown in this figure, the displacements from both approaches are within 1% of each other.

Figure 4(a) shows two engineering stress–strain curves for the above specimen, one constructed from the DIC displacements and the other from the Optical Flow displacements. Figure 4(b) shows a closeup of the linear regions and the 0.002 offset lines from the two analyses. The initial gauge width was measured from the optical micrographs while the initial gauge thickness was measured with a digital micrometer. As shown, the two curves are within 1% of each other. Table 2 compares the tensile properties obtained from both analyses. The DIC-derived tensile properties and their measurement uncertainties were reported in the previous studies [12]. The measured displacements factor into the following properties: the apparent Young's modulus, the 0.002 offset yield strength, and the elongation to fracture. The relative uncertainties were calculated using error analysis and were discussed in more detail in [29]. Since the absolute uncertainty in both programs is similar (0.2 pixels for DIC, 0.1 pixel for Optical Flow), the uncertainties in the tensile properties are similar when the images are analyzed with both approaches.

From table 2, there is a ∼9% discrepancy between the nominal values of the 0.002 offset yield strength between the Optical Flow and DIC-based measurements. As discussed in the previous study on the measurement uncertainties [29], the Young's modulus is the property with the largest uncertainty from a tensile test. Table 2 shows a ∼3% difference in the nominal values of Young's modulus between the Optical Flow and DIC analyses, which could be due to differences in how each program calculated small displacements such as those in the linear region of the stress–strain curve. Even though the stress–strain curves from Optical Flow and DIC are very similar as shown in figure 4(a), the 3% difference in Young's modulus leads to the 0.002 offset lines crossing the stress–strain curve at different locations in each case, as shown in the close up in figure 4(b). Given the nonlinearity of the stress–strain curve in the region of the yield stress, the 3% difference in slope of the 0.002 offset lines results in a 9% difference in the nominal values of the yield stress for the two cases. Nevertheless, this discrepancy in the yield stress is within the measurement uncertainty of 12%. [29] provides more details of the measurement uncertainties in the tensile tests which included the specimen in figure 4. Therefore, the Optical Flow method gives similar results to DIC for the mesoscale tensile specimen of nanocrystalline Ni-10% Fe in the current and previous study.

3.2. Mesoscale shear tests

In addition to the tensile properties, the in-plane shear properties of the two LIGA Ni alloys at similar size scale were also measured in previous studies [14]. The same test apparatus from the tensile tests was

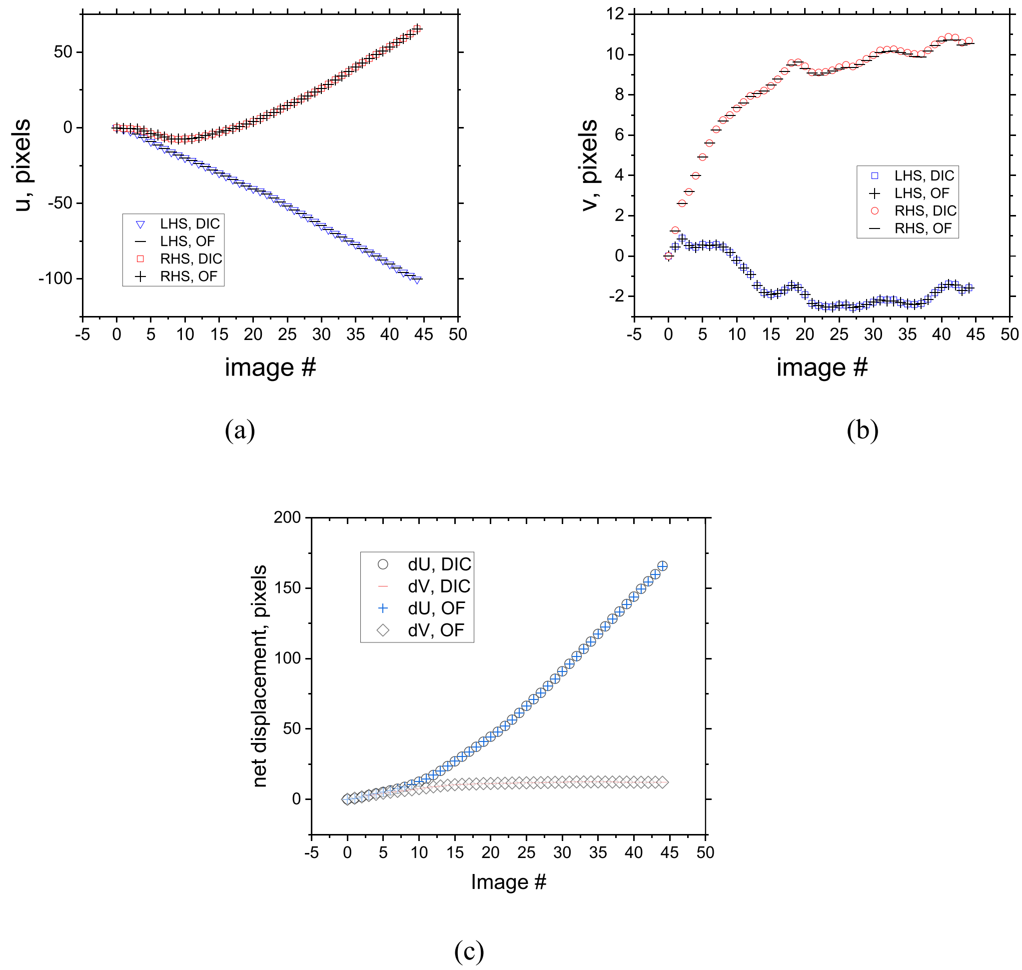

Figure 3. Raw displacements measured on the same set of images, using Optical Flow and DIC, for the mesoscale tensile test. The gauge section was 2000 pixels long. (a) Longitudinal displacements (stretch). (b) Transverse displacements (rigid body motion). (c) Net displacements in the x- and y-directions ('dU' and 'dV,' respectively) from DIC and Optical Flow.

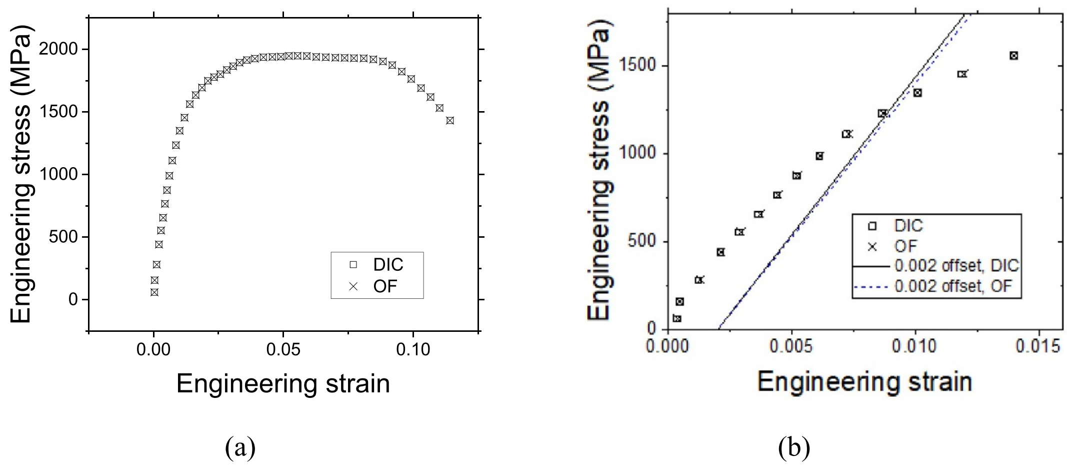

Figure 4. (a) DIC- and Optical Flow-derived engineering stress–strain curve for the 200 μm-thick tensile specimen of nanocrystalline Ni-10% Fe in figure 2, with gauge dimensions 200 μm wide × 2 mm long × 200 μm thick. (b) Close up of the stress–strain curves in (a) with the 0.002 offset lines.

used, and the images were analyzed with the same DIC program. One specimen of the ductile 200 μm thick Ni-10% Co alloy was reanalyzed in the present study using Optical Flow. Figure 5 shows optical micrographs of the gauge section during a shear test. For both DIC and Optical Flow analyses, an array

Table 2. Comparison of the tensile properties of one specimen of 200 μm-thick electrodeposited nanocrystalline Ni-10% Fe, based on the engineering stress–strain curve constructed from the DIC displacements and the Optical Flow displacements. The uncertainties are the measurement uncertainties derived from error analysis.

	DIC	Optical Flow
Ultimate tensile strength (MPa)	1947 ± 2%	1947 ± 2%
Apparent Young's modulus (GPa)	180 ± 12%	175 ± 12%
0.002 offset yield strength (MPa)	1233 ± 12%	1348 ± 12%
Engineering strain at UTS	0.0555 ± 2%	0.0555 ± 2%
Engineering strain at fracture	0.114 ± 2%	0.114 ± 2%

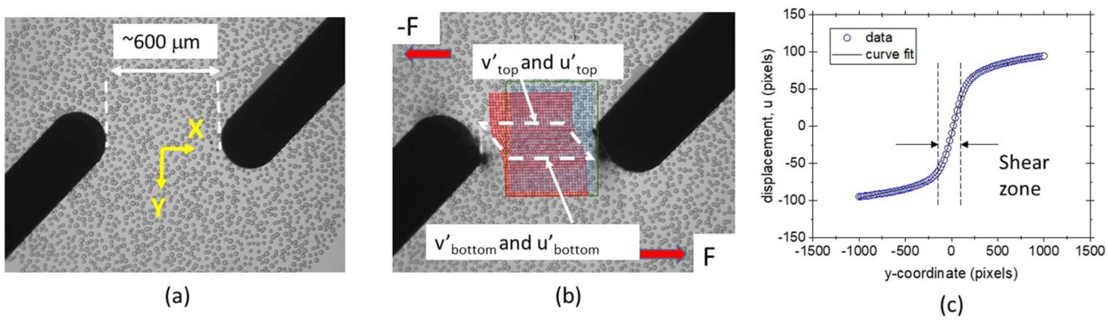

Figure 5. (a) Optical micrograph of an undeformed gauge section of a 200 μm-thick mesoscale shear specimen of micrograined electrodeposited Ni-10% Co. The dots are 1 μm-thick Au and serve as fiducial markers. (b) Optical micrograph of the deformed gauge section during the shear test, with the DIC grid overlayed. The trapezoid is manually drawn to represent the shear zone and is intended for illustrative purposes only. (c) Typical plot of measured displacement in the horizontal direction, u, as a function of the vertical position along the center of the gauge section, y_0. Reproduced from [14], with permission from Springer Nature, this caption is original.

of subsets was used to measure the displacements, u, in the x-direction, which is the direction of shear, as well as the transverse displacements, v, in the y-direction. The images were 3072 × 2300 pixels. For each image captured during the test, we plot u against y_0 for the central column of the array, where y_0 are the initial y-coordinates of each subset, figure 5(c) shows a typical plot. The simple shear strain is the slope of the linear segment of the sigmoidal curve in figure 5(c), which corresponds to the shear zone, and is calculated by fitting a hyperbolic tangent function to the sigmoidal curve [14].

The DIC and Optical Flow analyses both used subset sizes of 100 pixels and an array with 85 rows and 33 columns. The step size (distance between the centers of the subsets) was 25 pixels for the DIC program, and 26.19 pixels for the Optical Flow program due to sub-sampling. The y_0 of the first row was identical for the Optical Flow and DIC arrays, but the 4.75% larger step size used in the Optical Flow program (26.19 pixels as opposed to 25 pixels for DIC) resulted in each subsequent row being located at a slightly higher y-coordinate than its counterpart in the DIC array, shown in figure 6(a) which plots the y_o of each row in the subset array. For a given image, the calculated shear strain is the slope of the shear zone (i.e. the linear segment of the sigmoidal curve in figure 5(c)) and is unchanged by the slightly larger step size in the Optical Flow analysis since the slope is linear. Figure 6(b) shows the displacements u for the top and bottom rows of the array. The measured displacements were then used to calculate the specimen's rotation angle using equation (1):

$$\theta = \frac{1}{2}\left(\frac{\partial u}{\partial y} - \frac{\partial v}{\partial x}\right) \tag{1}$$

Figure 6(c) shows that the maximum rotation angle was under 2 degrees for both the DIC and Optical Flow analyses, with the discrepancy between the analyses being less than 1 degree.

A rotation angle under 1 degree, which was measured on this shear specimen and others of identical geometry [14], is experimentally negligible because the resultant force and displacement in the direction of shear differ by 1% or less from the total values measured along the x-axis. Nevertheless, we applied a rotation correction to all the displacements, as well as to the measured forces, to construct the shear stress vs shear strain curve for this specimen.

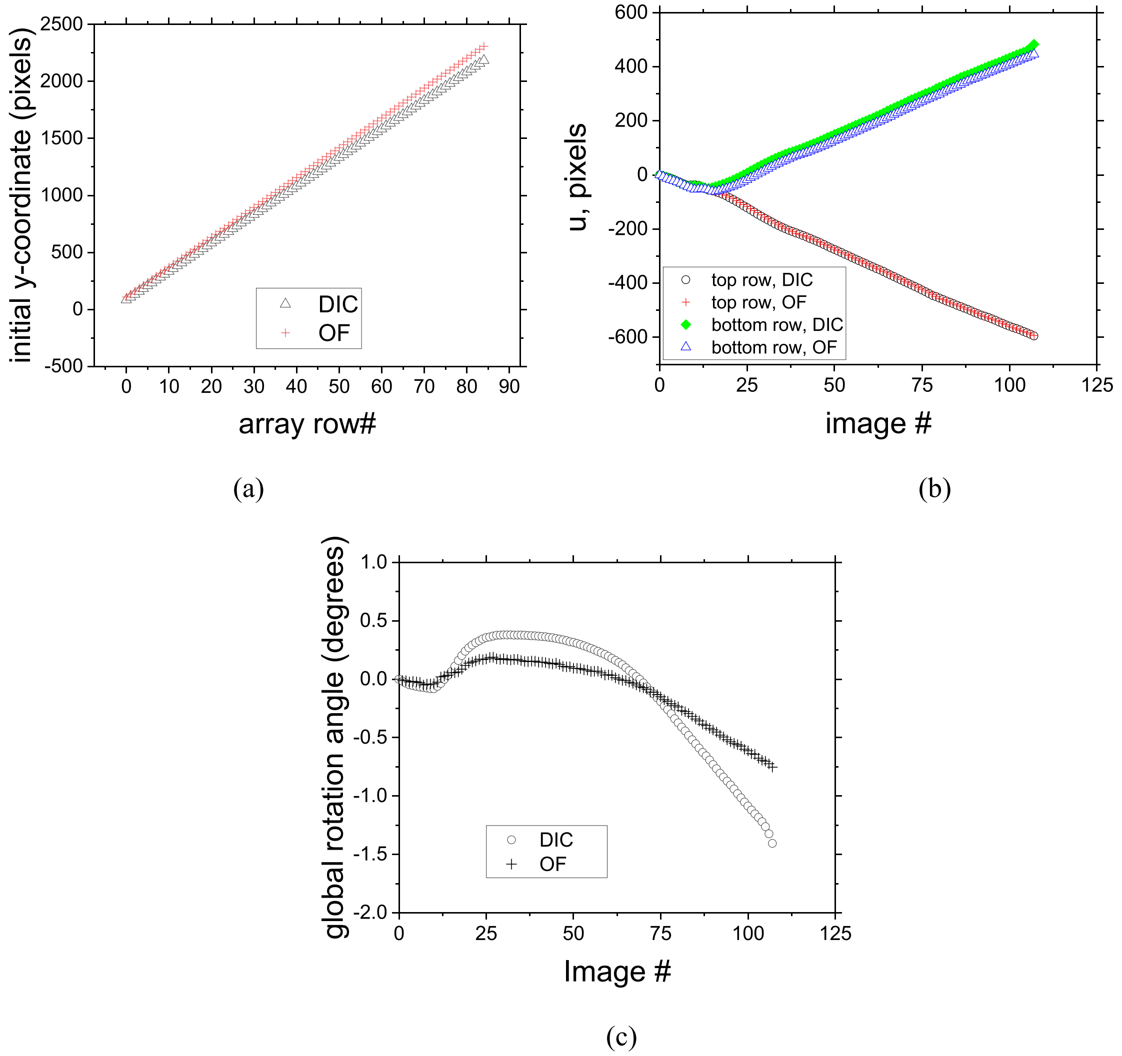

Figure 6. DIC and Optical Flow displacements, for one mesoscale shear specimen of 200 μm-thick Ni-10% Co. (a) Initial y-coordinates of the center column for each row in the subset array. The step size was 25 pixels for the DIC analysis and 26.19 pixels for the OF analysis. (b) Raw displacements in the x-direction, of the top and bottom row of the subset array. The displacements are for the center column of the subset array. (c) Specimen rotation angle during the shear test, calculated from the DIC and Optical Flow displacements. For both approaches, the absolute value of the maximum rotation angle is less than 1.5 degrees.

Figure 7 shows images from the shear test. Figure 7(a) shows the specimen at the start of the test, figure 7(b) shows the specimen at maximum shear stress or τ_{max}, and figure 7(c) is the last image before fracture. From the previous work [14] it was found that due to the high ductility of the Ni-10% Co alloy and the lack of rotational constraint due to pin-loading of the specimen in the clevises, the shear tests for the ductile Ni-10% Co alloy are valid until the maximum shear stress (τ_{max}) is reached. This is because further loading beyond τ_{max} resulted in extensive distortion, 'tearing apart' of the gauge section, and rotational motion of the upper and lower halves of the specimen relative to each other, such that the specimen no longer undergoes simple shear deformation as shown in figure 7(c). The failure criterion for the ductile Ni-10% Co shear specimens is therefore τ_{max}.

As mentioned earlier, the simple shear strain is the slope of the linear segment of the sigmoidal curve in figure 5(c). The same curve fitting procedure was used on both sets of displacements (from DIC and Optical Flow) to calculate the shear strains. After τ_{max} is reached, typically at shear strains between 1.8–2.0, continuing the curve fitting procedure on subsequent displacements results in artificial values of shear strain that are not physically valid since the specimen is no longer undergoing simple shear, as mentioned earlier and in [14]. We analyzed all images until fracture, even in the non-valid regime of the test (beyond τ_{max}), as the large artificial strain values served as a qualitative measure of the ductility of the Ni-10% Co alloy compared with the stronger and more brittle nanocrystalline Ni-10% Fe alloy which underwent much less deformation and remained in simple shear until fracture at a shear strain of 0.42 [14].

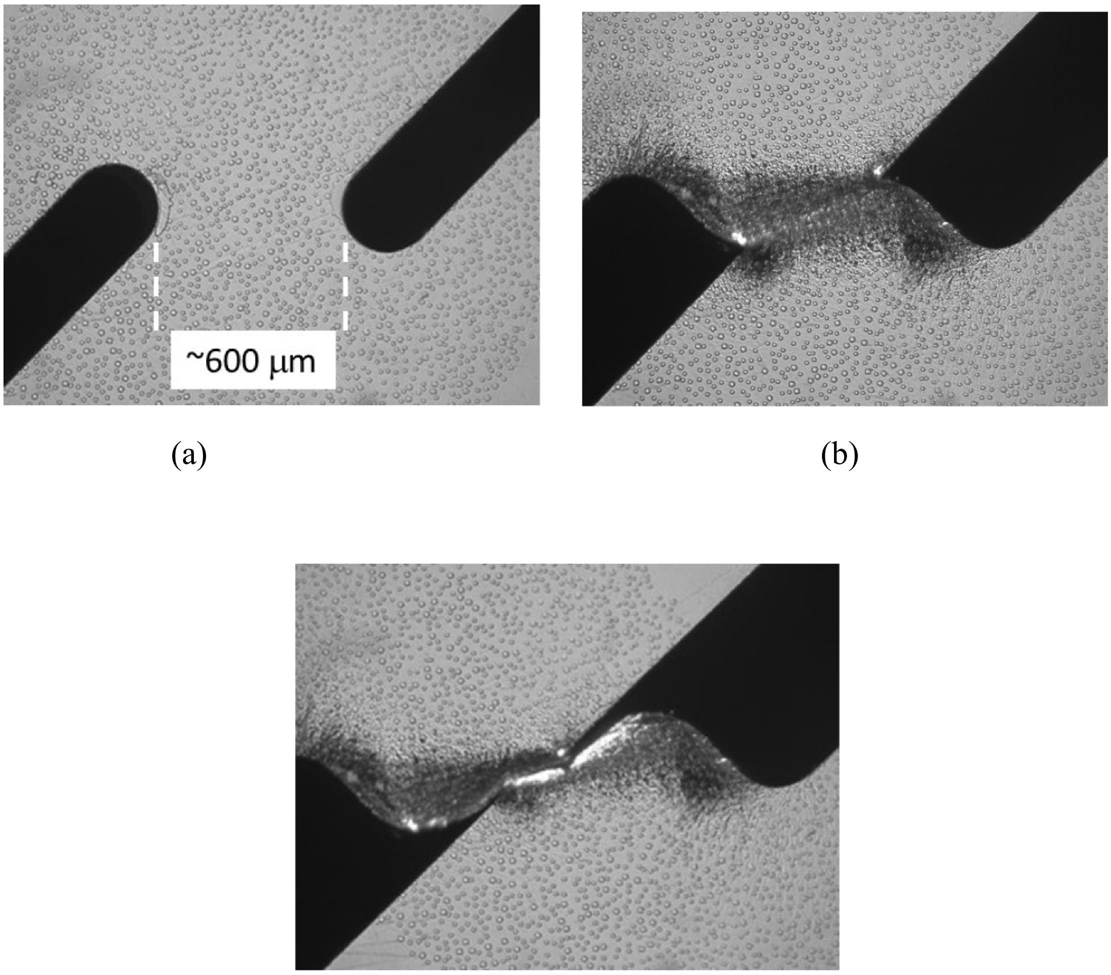

Figure 7. Optical micrographs from the shear test of the 200 μm-thick electrodeposited Ni-10% Co shear specimen in figures 6 and 8. (a) At the start of the test. (b) At the maximum shear stress, which is the failure criterion. (c) Just before fracture, showing extensive deformation and tearing, the deformation is no longer simple shear thus this portion of the shear test is experimentally invalid.

Figure 8 shows the shear stress vs shear strain curves constructed from the DIC and Optical Flow displacements for the Ni-10% Co specimen in figure 7, where the failure criterion is the maximum shear stress. The region to the left of the vertical line in figure 8(a) is the valid range of the test and is also shown in close up in figure 8(b). The shear strains to right of the vertical line in figure 8(a) are not physically valid but are still plotted until fracture.

Within the valid region of the test, shown in figure 8(b), the shear strains from DIC and Optical Flow are within 4%–9% of each other, with the larger discrepancy at the higher strains being outside the experimental uncertainty of 4%. This discrepancy between DIC and Optical Flow is larger than for the tensile specimen in the previous section, where the engineering strains were within 1% of each other and within the measurement uncertainty. This could be due to the fact that the tensile specimen was of the more brittle material (the nanocrystalline Ni-10% Fe alloy) and thus did not undergo as much change in surface texture and lighting contrasts during the test as the more ductile shear specimen in figure 7(b). The changes in surface texture and lighting in the shear test could have affected the DIC and Optical Flow programs differently, resulting in more variation in strain values between them than for the tensile specimen. These differences accumulated with increasing deformation when the shear specimen was loaded beyond $\tau_{\max}$ such that the artificial strain values (in the non-valid range of the test) from the two analyses increasingly deviated from each other to a final discrepancy of $\sim$20% just before fracture, as shown to the right of the vertical line in figure 8(a).

Changes in lighting and contrast from one image to another is a factor that affects both DIC and Optical Flow, though it can be corrected for to some degree depending on the choice of registration algorithm chosen. For example, the application of a bandpass filter to the image can reduce sensitivity to

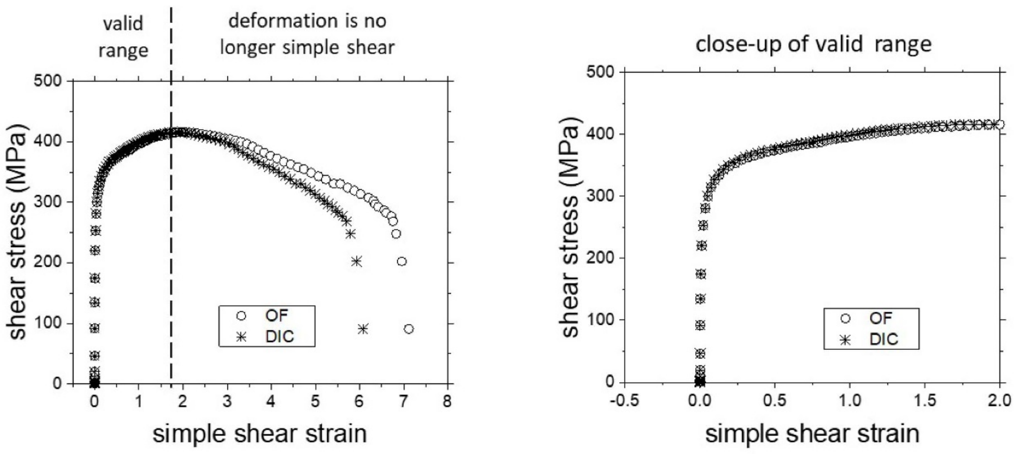

(a) (b)

Figure 8. (a) Engineering shear stress vs simple shear strain curves for the 200 μm thick specimen of electrodeposited Ni-10% Co in figures 6 and 7. The strains were computed separately from the DIC and Optical Flow displacements. The shear test is experimentally valid up to the maximum shear stress, indicated to the left of the vertical line. To the right of the vertical line, the ductile specimen is no longer in simple shear while continuing to be loaded until fracture, the calculated shear strains in this region are therefore not physically valid. (b) Close-up of the shear stress vs shear strain plot in (a) in the region of experimental validity, i.e. up to the maximum shear stress (failure criterion).

Table 3. Shear properties for one specimen of 200 μm-thick electrodeposited Ni-10% Co. The relative uncertainties are the measurement uncertainties derived from an error analysis. The failure criterion is the maximum shear stress (τ_{max}).

	DIC	Optical flow
Maximum shear strength, τ_{max} (MPa)	416 $\pm$ 1%	416 $\pm$ 1%
Shear modulus, G (GPa)	12 $\pm$ 9%	10 $\pm$ 9%
0.002 offset yield in shear (MPa)	250 $\pm$ 9%	250 $\pm$ 9%
Shear strain to τ_{max}	1.83 $\pm$ 4%	2.0 $\pm$ 4%

background lighting changes. Furthermore, because the DIC analysis used the first image as the reference whereas the Optical Flow analysis used the previous image, such discrepancies could have accumulated over more images and thus be larger at the end of the test.

Table 3 shows the shear properties obtained from the shear stress vs shear strain curves. As with the tensile test (table 2), the reported uncertainties were calculated from an error analysis and are independent of the number of specimens tested. Here we define the '0.002 offset yield in shear' as its analog in the tensile test, i.e. by constructing a straight line with slope equal to the shear modulus and offset by 0.002 strain on the shear stress–strain curve and then finding its intersection with the curve [14].

4. Discussion

The objective of this paper is to describe a case study where Optical Flow was found to provide similar results to traditional DIC for one mesoscale tensile test and shear test from previous work. For the shear test, the shear strains were within 4%–9% of each other until the failure criterion (τ_{max}) was reached. When the specimen was loaded beyond τ_{max} the discrepancy in artificial shear strain values increased to 20%. These discrepancies could be due to the ductile Ni-10% Co specimen exhibiting changes in surface texture and lighting which could have affected the two programs differently, with such differences accumulating with increasing deformation. For the less complex tensile specimen made from the more brittle Ni-10% Fe alloy, the engineering strains from both analyses were within 1% until fracture as the surface texture and lighting did not change as much during the tensile test. The results for these two specimens, while preliminary, suggest that Optical Flow is a promising method for strain measurement for the current mesoscale specimens. While the intent is not to replace DIC, the Optical Flow approach in general has certain advantages over traditional DIC, which make it a promising approach for further study. Following is a more general discussion of factors affecting Optical Flow and traditional DIC.

The choice of algorithm for measuring strain, whether it is some version of DIC or Optical Flow, can be seen as a balance between accuracy, robustness [36] and computational efficiency. Accuracy is limited by the equipment used, the correlation calculation chosen, bit depth of numerical representation, and the type of interpolation, if any, used to achieve sub-pixel accuracy [30, 34]. Robustness refers to an algorithm's ability to continue tracking under less than ideal or changing conditions. For DIC, consideration must be given to whether lighting conditions might change, the amount of time or deformation expected between frames, and the amount of total deformation expected. Efficiency becomes more important as the size, pixel density, and number of images to be analyzed increases.

A pyramidal implementation of the Lucas–Kanade feature tracker using Optical Flow provides a balance between accuracy, robustness, and computational efficiency. The incorporation of a velocity component to estimate the likely location of each image segment along with a pyramidal approach to correlation potentially allows registration of segments between frames more efficiently than the simple hill climbing, subsection search used in our older DIC implementation. As long as movement of segments is consistent enough that the velocity-based estimate is accurate, this method can potentially reduce the search area considerably while also allowing greater displacements between frames without loss of tracking. For more information on the efficiency of various correlation criteria, please refer to [38, 39].

The use of a predictive location search also lowers the possibility that the registration algorithm might mistakenly identify a region with a similar brightness pattern, in an incorrect area of the target image, as the segment to be tracked. The difficulties in creating DIC-suitable speckle patterns on micro- and mesoscale specimens if the surface texture is not sufficient are well-documented and motivated the use of microengineered fiducial markers in the present specimens [13]. With microengineered fiducial markers the pattern is well controlled and repetition can be avoided, making erroneous region identification unlikely with either algorithm. However, the predictive location functionality of Optical Flow and its subsequent lower probability of erroneous region identification (compared to traditional DIC) could be beneficial for testing specimens with a less controllable speckle pattern. For example, speckle patterns produced with spray paint can inadvertently create small sub-regions with similar speckle patterns that can potentially be misidentified. In addition, for other ductile mesoscale specimens similar to those in this study, the Optical Flow method maintained its ability to track segments under lighting conditions and deformations that were beyond the capability of the older traditional DIC implementation.

Traditional DIC algorithms often search for image segments by comparing template subsections from the first image to each subsequent frame. This strategy tends to give a slightly more accurate result over long image sequences because it does not allow for frame-to-frame drift of the template image. Optical Flow does not lend itself to this type of comparison because subset velocities are calculated on a frame-to-frame basis. The pixel brightness values to be tracked in each frame are taken from the calculated locations of the segments of the previous frame. In a well-conducted tensile or shear test there is typically very little difference in the brightness values of segments from frame to frame unless there is large deformation in the underlying sample. Continuous updating of the segment being matched, combined with the additional location prediction step, could potentially allow the Optical Flow algorithm to continue tracking regions that the DIC algorithm cannot, as we informally observed in other mesoscale specimens of the same alloys which were not included in the present case study. If the image brightness template is rapidly evolving from frame to frame, then the optical flow method may maintain its tracking at the cost of introducing small cumulative errors in the calculated motion.

The field of computer vision is rapidly advancing, and new innovations in both DIC and Optical Flow are happening regularly. In this study, we chose to use a pyramidal implementation of the Lucas–Kanade Optical Flow algorithm [36] to compare with previously published data obtained using a traditional DIC algorithm [12, 14]. More modern Optical Flow implementations based on convolutional neural networks have been developed [40, 41] and are extending the field of computer vision. To date they are not commonly used in the field of mechanical testing. Neural networks require extensive training and a data set of ground truth examples which, for this case study, were not possible to generate using the available data. To do so in the present work, we would have had to either train the neural network on the previous DIC data, or rely on generalized training that was not directly applicable to our use case, which could lower the accuracy of the neural network. The use of the more traditional Optical Flow implementation in this work helps to ensure that all calculation steps are knowable, and that the data used is only from the sample under test.

5. Conclusions

We described a case study where Optical Flow was applied to deformation measurements of two mesoscale specimens of electrodeposited Ni alloys, and the results compared with previously published results from a traditional DIC approach. The predictive velocity component and pyramidal search used in Optical Flow provided acceptable accuracy along with increased robustness and qualitatively lower computation time. The tensile and in-plane shear properties of 200 μm-thick films of electrodeposited LIGA nickel alloys, for MEMS applications, were measured from the same set of images using Optical Flow and DIC. The raw displacements, engineering stress–strain curves, shear stress–strain curves, and the materials' tensile and shear properties extracted from the curves, were compared from the two approaches. The engineering strains for the tensile specimen of the Ni-10%Fe alloy were within 1% of each other, and the shear strains of the more ductile Ni-10% Co alloy were within 4%–9% of each other until the failure criterion of $\tau_{\max}$. We also discussed general advantages of Optical Flow over traditional DIC, such as faster run time and the potential for less reliance on the speckle pattern quality, a feature which could be especially beneficial for micro- and mesoscale mechanical test specimens due to the well-documented general difficulties in speckle pattern creation at this size scale. Thus, this case study suggests that Optical Flow shows promise as a tool for displacement measurement in the testing of micro- and mesoscale specimens and warrants further study with more specimens.

Acknowledgments

The authors thank Dr David Read, Dr Jeffrey Smyth and Mr. John Geaney for valuable discussions. Specific commercial equipment, instruments, and materials that are identified in this report are listed in order to adequately describe the experimental procedure and are not intended to imply endorsement or recommendation by the National Institute of Standards and Technology (NIST). This work was funded by the U.S. Army DEVCOM Armaments Center and the Joint Fuze Technology Program (JFTP). The JFTP project number was 14-G-006, Micro Scale Materials and Energetic Effects Characterization (principal investigator Mr. John Geaney), and JFTP 19-G-018 Fracture and Damage Mechanisms of Electrodeposited LIGA Nickel Alloys (principal investigator Dr. Jeffrey Smyth). This work was also partially funded by the CHIPS Metrology Program, part of CHIPS for America, National Institute of Standards and Technology, U.S. Department of Commerce.

Data availability statement

No new data were created or analysed in this study.

Funding

This work was funded by the U.S. Army DEVCOM Armaments Center and the Joint Fuze Technology Program (JFTP). The JFTP project number was 14-G-006, Micro Scale Materials and Energetic Effects Characterization (principal investigator Mr. John Geaney), and JFTP 19-G-018 'Fracture and Damage Mechanisms of Electrodeposited LIGA Nickel Alloys' (principal investigator Dr Jeffrey Smyth). This work was also partially funded by the CHIPS Metrology Program, part of CHIPS for America, National Institute of Standards and Technology, U.S. Department of Commerce.

Conflict of interest

The authors declare that they have no known competing financial or non-financial interests that could have appeared to influence the work reported in this paper.

Compliance with ethical standards

This work does not include studies on human subjects, human data or tissue, or animals.

Data access

The datasets generated and supporting the findings of this article are obtainable from the corresponding author upon reasonable request.

Author contributions

Damian Lauria 0000-0002-6338-1037
Conceptualization (lead), Investigation (lead), Methodology (lead), Software (lead), Validation (supporting), Visualization (lead), Writing – original draft (equal), Writing – review & editing (equal)

Li-Anne Liew 0000-0003-0202-026X
Formal analysis (lead), Funding acquisition (lead), Investigation (supporting), Methodology (supporting), Project administration (lead), Validation (lead), Writing – original draft (equal), Writing – review & editing (equal)

References

[1] Haque M A and Saif M T A 2003 A review of MEMS-based microscale and nanoscale tensile and bending testing *Exp. Mech.* **43** 248–55
[2] Hemker K J and Sharpe W N Jr 2007 Microscale characterization of mechanical properties *Annu. Rev. Mater. Res.* **37** 93–126
[3] Gianola D S and Eberl C 2009 Micro- and nanoscale tensile testing of materials *JOM* **61** 24–35
[4] Ast J, Ghidelli M, Durst K, Göken M, Sebastiani M and Korsunsky A M 2019 A review of experimental approaches to fracture toughness evaluation at the micro-scale *Mater. Des.* **173** 107762
[5] Borasi L, Slagter A, Mortensen A and Kirchlechner C 2025 On the preparation and mechanical testing of nano to micron-scale specimens *Acta Mater.* **283** 120394
[6] Bardelcik A and Butler Q 2024 Strain partitioning characterization of advanced high strength steels using *in-situ* tensile tests with Micro digital image correlation—methodology and analysis *Mater. Charact.* **218** 114451
[7] Stöckel S and Groeger S 2025 Fiducial markers for image alignment of surface texture measurements *Surf. Topogr. Metrol. Prop.* **13** 035011
[8] Becker E W, Ehrfeld W, Hagmann P, Maner A and Münchmeyer D 1986 Fabrication of microstructures with high aspect ratios and great structural heights by synchrotron radiation lithography, galvanoformung, and plastic moulding (LIGA process) *Microelectron. Eng.* **4** 35–36
[9] Ehrfeld W 1990 The LIGA process for microsystems *Micro System Technologies* Vol. 90 H Reichl ed (Springer)
[10] Guckel H, Christenson T R, Skrobis K J, Denton D D, Choi B, Lovell E.G., Lee J W, Bajikar S S and Chapman T W 1990 Deep x-ray and UV lithographies for micromechanics *IEEE 4th Technical Digest on Solid-State Sensor and Actuator Workshop* (*Hilton Head Island, SC*) pp 118–22
[11] Christenson T R and Guckel H 1995 Deep x-ray lithography for micromechanics *Proc. SPIE* **2639** 134–45
[12] Liew L-A, Read D T, Martin M L, DelRio F W, Bradley P E, Barbosa N, Christenson T and Geaney J 2020 Elastic-plastic properties of mesoscale electrodeposited LIGA nickel alloy films: microscopy and mechanics *J. Micromech. Microeng.* **31** 015002
[13] Liew L-A, Read D T, Martin M L, Christenson T R and Geaney J 2021 Microfabricated fiducial markers for digital image correlation-based micromechanical testing of LIGA Ni alloys *Eng. Res. Express* **3** 025019
[14] Liew L-A, Read D T, Martin M L, Christenson T R, Bradley P E, Barbosa N, DelRio F W, Geaney J G and Smyth J R 2021 Experimental study of shear and tensile properties of LIGA Ni-Fe and Ni-Co alloys at quasi-static and intermediate strain rates *Mechanics of Biological Systems and Materials & Micro- and Nanomechanics & Research Applications* (Springer) (https://doi.org/10.1007/978-3-030-59765-8_19)
[15] Martin M L, Liew L-A, Read D T, Christenson T R, DelRio F W and Geaney J G 2020 Dominant factors for fracture at the micro-scale in electrodeposited nickel alloys *Sensors Actuators A: Physical* **314** 112239
[16] Read D T, Liew L A, White R M, Barbosa N and Geaney J 2019 Measuring flow curve and failure conditions for a MEMS-scale electrodeposited nickel alloy *Mater. Res. Express* **6** 0950a6
[17] Benzing J T, Liew L A, Hrabe N and DelRio F W 2020 Tracking defects and microstructural heterogeneities in meso-scale tensile specimens excised from additively manufactured parts *Exp. Mech.* **60** 165–70
[18] Watring D S, Benzing J T, Kafka O, Liew L-A, Moser N H, Erickson J, Hrabe N and Spear A D 2022 Evaluation of a modified void descriptor function to uniquely characterize pore networks and predict fracture-related properties in additively manufactured metals *Acta Mater.* **223** 117464
[19] Sharpe W N Jr 1982 Applications of the interferometric strain/displacement gage *Opt. Eng.* **21** 483–8
[20] Sutton M A, Orteu J J and Schreier H 2009 *Image Correlation for Shape, Motion and Deformation Measurements: Basic Concepts, Theory and Applications* (Springer) (https://doi.org/10.1007/978-0-387-78747-3)
[21] Pan B 2011 Recent progress in digital image correlation *Exp. Mech.* **51** 1223–35
[22] Luo P F, Chao Y J, Sutton M A and Peters W H 1993 Accurate measurement of three-dimensional deformations in deformable and rigid bodies using computer vision *Exp. Mech.* **33** 123–32
[23] Chivers K and Clocksin W 2000 Inspection of surface strain in materials using optical flow. *Proc. British Machine Vision Conf.* (BMVA Press) pp 41.1–41.10
[24] Hartmann C, Wang J, Opristescu D and Volk W 2018 Implementation and evaluation of optical flow methods for two-dimensional deformation measurement in comparison to digital image correlation *Opt. Lasers Eng.* **107** 127–41

[25] Hartmann C and Volk W 2019 Digital image correlation and optical flow analysis based on the material texture with application on high-speed deformation measurement in shear cutting *Int. Conf. on Digital Image & Signal Processing* (*United Kingdom*)
[26] Luo Z, Hu X, Wang L and Lu Y 2020 Measurement of large, discontinuous displacement from digital images *Strain* **56** e12349
[27] Zhang Y, Yan L, Karnati S and Liou F 2019 Bisection searching based reference frame update strategy for digital image correlation *SN Appl. Sci.* **1** 588
[28] Pan B, Dafang W and Yong X 2012 Incremental calculation for large deformation measurement using reliability-guided digital image correlation *Opt. Lasers Eng.* **50** 586–92
[29] Liew L-A, Read D T, Martin M L, Bradley P E and Geaney J T 2023 Elastic-plastic properties of mesoscale electrodeposited LIGA nickel alloy films: analysis of measurement uncertainties *J. Verification, Validation and Uncertainty Quantification* **8** 011005
[30] Read D T, Cheng Y-W, Sutton M A, McNiell S R and Schreier H 2001 Proposed standardization effort: digital-image correlation for mechanical testing *Proc. SEM Annual Conf Exp. App. Mech.* (*Portland, OR*) pp 365–8 (available at: https://tsapps.nist.gov/publication/get_pdf.cfm?pub_id=851184)
[31] Marquardt D W 1963 An algorithm for least-squares estimation of nonlinear parameters *J. Soc. Ind. Appl. Math.* **11** 431–41
[32] Levenberg K 1944 A method for the solution of certain non-linear problems in least squares *Q. Appl. Math.* **2** 164–8
[33] Ranganathan A 2004 The levenberg-marquardt algorithm *Tutoral on LM algorithm* **11** 101–10 (available at: https://citeseerx.ist.psu.edu/viewdoc/download?doi=10.1.1.135.865&rep=rep1&type=pdf)
[34] Lucas B D and Takeo K 1981 An iterative image registration technique with an application to stereo vision *Proc. DARPA Image Understanding Workshop* pp 121–30 (available at: www.ri.cmu.edu/pub_files/pub3/lucas_bruce_d_1981_2/lucas_bruce_d_1981_2.pdf)
[35] Pan B, Qian K, Xie H and Asundi A 2009 Two-dimensional digital image correlation for in-plane displacement and strain measurement: a review *Meas. Sci. Technol.* **20** 062001
[36] Bouguet J-Y 2001 Pyramidal implementation of the affine lucas kanade feature tracker description of the algorithm *Intel corporation* (available at: http://robots.stanford.edu/cs223b04/algo_affine_tracking.pdf)
[37] Horn B K P and Schunck B G 1981 Determining optical flow *Artif. Intell. MIT Artif. Intell. Lab A.I. Memo No.* vol 572 pp 185–203 (available at: https://dspace.mit.edu/bitstream/handle/1721.1/6337/%EE%80%80AIM%EE%80%81-572.pdf?sequence=2)
[38] Pan B, Xie H and Wang Z 2010 Equivalence of digital image correlation criteria for pattern matching *Appl. Opt.* **49** 5501–9
[39] Baker S and Matthews I 2004 Lucas-Kanade 20 years on: a unifying framework *Int. J. Comput. Vis.* **56** 221–55
[40] Dosovitskiy A, Fischer P, Ilg E, Hausser P, Hazırbas C, Golkov V, van der Smagt P, Cremers D and Brox T 2015 FlowNet: learning optical flow with convolutional networks 2015 *IEEE Int. Conf. on Computer Vision (ICCV)* (*Santiago, Chile*) pp 2758–66
[41] Teed Z and Deng J 2020 RAFT: recurrent all-pairs field transforms for optical flow *Proc. 16th European conf. on computer vision (ECCV 2020)* (*Glasgow, UK*) pp 402–19